RSC Advances

PAPER

View Article Online
View Journal | View Issue

Cite this: *RSC Adv.*, 2015, **5**, 15923

Pt nanoparticles on tin oxide based support as a beneficial catalyst for oxygen reduction in alkaline solutions

N. R. Elezovic,*[a] V. R. Radmilovic,[b] J. Kovac,[c] B. M. Babic,[d] Lj. M. Gajic-Krstajic[e] and N. V. Krstajic[b]

A platinum nanocatalyst on Sb doped tin oxide support (Sb–SnO_2) was synthesized and characterized as a catalyst for oxygen reduction reaction in 0.1 mol dm^{-3} NaOH solution at 25 °C. Sb (5%) doped tin oxide support was synthesized by a modified hydrazine reduction procedure. The platinum nanocatalyst (20% Pt) on Sb–SnO_2 support was synthesized by a borohydride reduction method. The synthesized support and catalyst were characterized by high resolution transmission electron microscopy (HRTEM) and X-ray photoelectron spectroscopy (XPS) and X-ray diffraction technique (XRD). X-ray photoelectron spectroscopy was applied to characterize the chemical status of elements before and after Pt-treatment. XPS spectra of Sn 3d, Pt 4f, Sb 3d and O 1s revealed that the Pt-deposition on Sb–SnO_2 support induced the reduction of the Sn(4+) oxidation state to Sn(2+) and Sn(0) states, while Pt remained in the metallic state and Sb was in the (3+) oxidation state. Homogenous Pt nanoparticle distribution over the support, without pronounced particle agglomeration, was confirmed by HRTEM technique. The average Pt particle size was 2.9 nm. The electrochemically active Pt surface area of the catalyst was determined by the integration of the cyclic voltammetry curve in the potential region of underpotential deposition of hydrogen, after double layer charge correction, taking into account the reference value of 210 μC cm^{-2} for full monolayer coverage. This calculation gave the value of 51 m^2 g^{-1}. The kinetics of the oxygen reduction reaction with Pt/Sb–SnO_2 catalyst was studied by cyclic voltammetry and linear sweep voltammetry using a rotating gold disc electrode. Two different Tafel slopes were observed: one close to 60 mV dec^{-1} in the low current density region, and another at ~120 mV dec^{-1} in the higher current densities region, as was already referred in previous reports for the oxygen reduction reaction with polycrystalline Pt, as well as with different Pt based nanocatalysts. The specific activities for oxygen reduction, expressed in terms of kinetic current densities per electrochemically Pt active surface area, as well as per mass of Pt loaded, at the constant potential of practical interest (0.85 V and 0.90 V *vs.* RHE), were compared to a carbon supported (Vulcan XC-72) catalyst. The Pt/Sb–SnO_2 catalyst exhibited similar catalytic activity for oxygen reduction reaction like carbon supported one. The advantages of the carbon free support application in terms of the durability and stability of the catalysts were proved by accelerated stability tests.

Received 30th October 2014
Accepted 19th January 2015

DOI: 10.1039/c4ra13391a

www.rsc.org/advances

1. Introduction

Alkaline electrolysis has been a subject of interest mainly due to chlorine alkali electrolysis and new developments in alkaline fuel cells. Although alkaline fuel cells have successful operation in space applications, they have not been used extensively due to the problems caused by electrolyte carbonation.[1,2] However, the recent development of a new type of membrane, characterized by absence of metal cations, which is crucial for the elimination of carbonate precipitation, again gave a perspective for alkaline fuel cell investigations.[3]

It could be expected that the kinetics of oxygen reduction reaction in alkaline solution is generally faster than in acid solution. According to previous reports it can be attributed to a lower degree of specific anion adsorption.[1] As the adsorption of spectator ions inhibits many electrocatalytic processes, the decreased anion adsorption in alkaline media implies that most of electrocatalytic processes should be more facile in alkaline solutions than in acidic solutions.[4]

The other important advantage over aggressive acid electrolytes is the fact that with alkaline electrolytes less expensive electrode materials can be used. Only a few materials are stable

[a]*Institute for Multidisciplinary Research, University of Belgrade, Kneza Viseslava 1, Belgrade, Serbia. E-mail: nelezovic@tmf.bg.ac.rs*
[b]*Faculty of Technology and Metallurgy, University of Belgrade, Belgrade, Serbia*
[c]*Jozef Stefan Institute, Jamova 39, Ljubljana, Slovenia*
[d]*Vinča Institute of Nuclear Sciences, University of Belgrade, Serbia*
[e]*Institute of Technical Sciences of the Serbian Academy of Sciences and Arts, Knez Mihailova 35, Belgrade, Serbia*

under a strongly acidic environment, especially under the strongly oxidizing conditions encountered at oxygen cathodes.[1]

Recently, many non-noble catalysts were introduced as prospective candidates for alkaline fuel cell application. X. Li *et al.* investigated non-precious metal catalysts synthesized from the precursors of carbon, nitrogen and transition metal for oxygen reduction in alkaline fuel cells and showed comparable activity for oxygen reduction with Pt/C as benchmark catalyst.[5] A cobalt tetraferrocenylporphyrin catalyst onto modified graphene support was synthesized by a solvothermally assisted method and the results showed that this catalyst exhibited an outstanding electrocatalytic performance towards the ORR, which is comparable with commercial Pt/C catalyst in alkaline media.[6] The $NaCo_2O_4$/C cathode catalysts were prepared by a dry-up method and tested for oxygen reduction in alkaline solutions. The maximum power density of 27 mW cm^{-2} was obtained.[7] Nitrogen/sulfur co-doped carbon materials were investigated as non-precious metal catalysts for the ORR in alkaline media. The promising catalytic activity towards the ORR and 4-electron transfer pathway in 0.1 mol 0.1 KOH was revealed.[8] Metal N doped nanoporous carbon (N–M–nC, M = Fe, Co) was prepared by the *in situ* incorporation of metal during the formation of the nanoporous carbon skeleton followed by NH_3 treatment. It was shown that the performance of the catalyst is comparable to that of commercial Pt/C.[9] Nitrogen-doped graphene-supported Co/CoNx was referred to as a highly efficient electrocatalyst for oxygen reduction reaction in an alkaline medium as well.[10]

Platinum based catalysts are among the most active catalysts for oxygen reduction in alkaline solutions, from single crystals to nanoparticles on carbon support, owing to high catalytic activity and stability.[11–14] The problem of the catalysts' durability and stability, caused by carbon degradation, especially at high anodic potentials, was recognized.[15,16] In order to overcome this problem, Pt supported catalysts on metal oxides, such as Ti, Nb, Sn, were studied mainly in acidic solutions due to their potential for oxygen reduction.[17–21] SnO_2 belongs to the broad-band semiconductors, with relatively high electronic conductivity, however further increase in the conductivity of such oxides can be expected by doping with hypervalent or hypovalent ions such as Nb, Sb or Al.[22]

In this study, antimony doped tin oxide support was synthesized by modified hydrazine reduction and fully characterized by XRD, XPS and TEM techniques. A platinum nanoparticle based catalyst was synthesized onto this support. This catalyst was tested for oxygen reduction in alkaline solution. The aim of this study was to reveal the influence of the carbon free support on the Pt catalyst's performance. The obtained results were compared to a Pt catalyst on commercial carbon support – Vulcan XC-72. The advantages of this carbon free support in terms of durability and stability at high anodic potentials were proved experimentally by accelerated stability tests.

2. Experimental

2.1. Preparation of the Sb–SnO_2 support and Pt/Sb–SnO_2 catalyst

Antimony doped SnO_2 support was synthesized by modified hydrazine reduction procedure.[23] The synthesis implies reduction of $SnCl_4$ and $SbCl_3$ acid solution by hydrazine. Details are given in ref. 24. Pt nanocatalyst on Sb–SnO_2 support was synthesized by the borohydride reduction method.[25] The Pt/Vulcan catalyst, used as a benchmark, was synthesized on commercial Vulcan XC-72 support.

2.2. Support and catalyst physical–chemical characterization

The synthesized support and catalyst were characterized by X-ray diffraction technique, X-ray photoelectron spectroscopy and transmission electron microscopy.

High angle annular dark field (HAADF), bright field (BF), and electron energy loss spectroscopy (EELS) techniques in a scanning transmission electron microscope (STEM) were applied for measuring the surface properties of the supports and catalysts. TEM characterization was performed at the National Center for Electron Microscopy NCEM-Berkeley, Lawrence Berkeley National Laboratory. Details related to the TEM measurements experimental procedure are described in ref. 24.

The X-ray photoelectron spectroscopy (XPS or ESCA) analyses were carried out on the PHI-TFA XPS spectrometer produced by Physical Electronics Inc. Sample powders were deposited on vacuum compatible carbon adhesive tape and introduced into the ultra-high vacuum spectrometer. The analyzed area was 0.4 mm in diameter and the analyzed depth was about 3–5 nm. This high surface sensitivity is a general characteristic of the XPS method. Sample surfaces were excited by X-ray radiation from monochromatic Al source at the photon energy of 1486.6 eV. The high-energy resolution spectra were acquired with an energy analyzer operating at a resolution of about 0.6 eV and pass energy of 29 eV. During data processing the spectra from the surface were aligned by setting the C 1s peak at 284.8 eV, which is a characteristic for the C–C bond. The accuracy of binding energies was about $\pm$0.2 eV. Two different XPS measurements were performed on each sample in order to check the homogeneity and reproducibility of acquired spectra, both of which were very high.

2.3. Electrochemical characterization

All electrochemical experiments were performed in a standard three electrode electrochemical cell, at the rotating disc electrode in 0.1 mol dm^{-3} electrolyte, prepared using 18.2 MΩ pure water, at the temperature of 25 °C. The counter electrode was a 5 cm^2 surface area Pt sheet, whereas a platinum plated Pt reversible hydrogen electrode (RHE) in the same solution and at the same temperature was applied as the reference electrode. The working electrode was a gold rotating disk (diameter 5 mm). The catalyst ink was prepared as a suspension of the catalyst in ethanol and Nafion solution (5 wt% Aldrich solution). It was ultrasonically dispersed for 30 min. An aliquot of ink was transferred on the gold electrode and dried at 80 °C for 10 min to obtain a thin film. The Pt loading was 8 μg of Pt – 40 μg cm^{-2}, expressed per geometric surface area. Electrochemical measurements were performed using a potentiostat/galvanostat PAR Model 273.

3. Results and discussion

3.1. XRD, XPS and HRTEM results

An X-ray diffraction pattern of Sb–SnO_2 support is presented in Fig. 1. The characteristics peaks of SnO_2 are present: (110) at $2\theta = 26.60$, (101) at $2\theta = 33.80$, (211) at $2\theta = 51.70$, and (112) at $2\theta = 64.70$. The peaks in the XRD patterns are associated to the rutile structure of SnO_2 (cassiterite). The diffraction peaks belonging to Sb species or compounds were not detected. The reason for the absence of antimony based compounds in the XRD pattern could be low Sb content, close to detection level for X-ray diffraction. The possible reasons could be the small particle size and the non-crystalline form of Sb compounds in the support powders, as well as quasi amorphous structure.

The average crystallite size can be calculated from the Scherrer equation,

$$D = \frac{0.9\lambda_{K\alpha_1}}{B_{2\Theta}\cos\Theta_{max}} \quad (1)$$

where $\lambda_{K\alpha_1}$ is the X-ray wave length (0.154 nm, for Cu $K\alpha_1$ radiation), $B_{2\Theta}$ is the width of the diffraction peak at half height (rad) and Θ_{max} is the angle at the position of the peak maximum. The average crystallite size of 3 nm was determined for the Sb–SnO_2 support.

Fig. 2a shows the XPS core lever spectra of Sb 3d. On the Sb–SnO_2 sample, the Sn $3d_{5/2}$ peak is at 487.3 eV. It can be assigned to the Sn(4+) in SnO_2.

On the Pt/Sb–SnO_2 sample, the Sn $3d_{5/2}$ spectra were significantly different from that on the Sb–SnO_2 and were fitted with three components (Fig. 2b). The main component at 487.2 eV is related with the Sn(4+) state and it is about 65% of the relative intensity of the total Sn 3d signal. The second component is at 486.3 eV and it may be related with the reduced Sn(2+) state.[26,27] It is about 30% of the relative intensity of the Sn 3d signal. The third component is at 485.3 eV and it is related to metallic Sn(0). The last component is about 5% of the relative intensity of the total Sn 3d signal. The main result of the XPS method is that the reduction of Sn took place during Pt-treatment and the reduced SnO_x is stable after treatment.

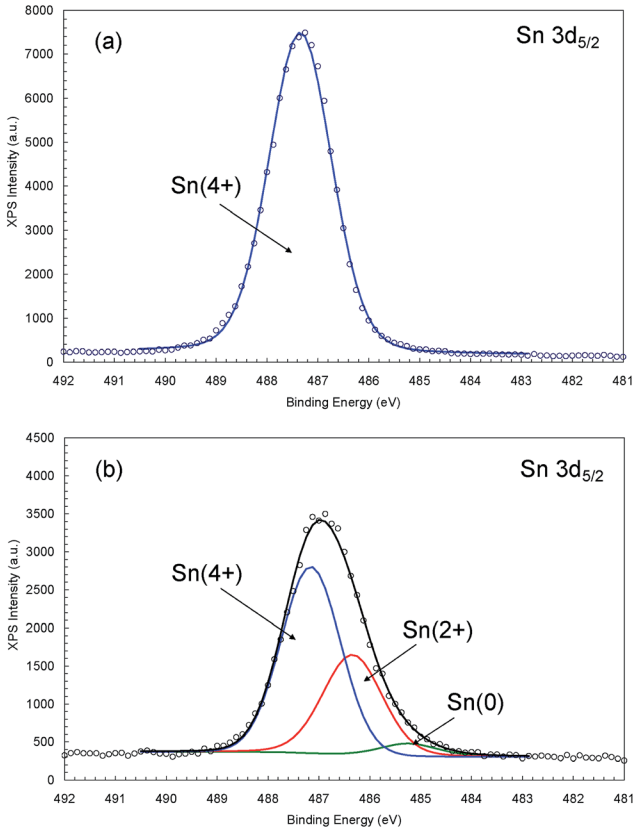

Fig. 2 XPS spectra of the Sn $3d_{5/2}$ obtained on the Sb–SnO_2 sample (a), Pt/Sb–SnO_2 sample (b).

Fig. 3 shows the Pt 4f spectra from Pt/Sb–SnO_2 sample. It consists of doublets of Pt $4f_{7/2}$ and $4f_{5/2}$ at binding energies of 70.8 eV and 74.1 eV, respectively. Spectra are asymmetric towards the high binding energy side. The binding energy and spectra shape show that Pt is present mainly in the metallic form.[26–28] Some other oxidation states of Pt can not be completely ruled out due the noisy spectra related to the very low concentration of Pt (about 1 at%) in the treated Sb–SnO_2

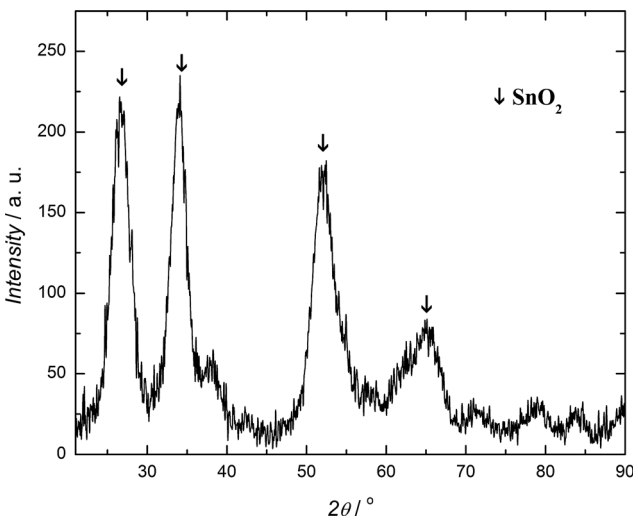

Fig. 1 X-ray diffraction pattern for the Sb–SnO_2 support.

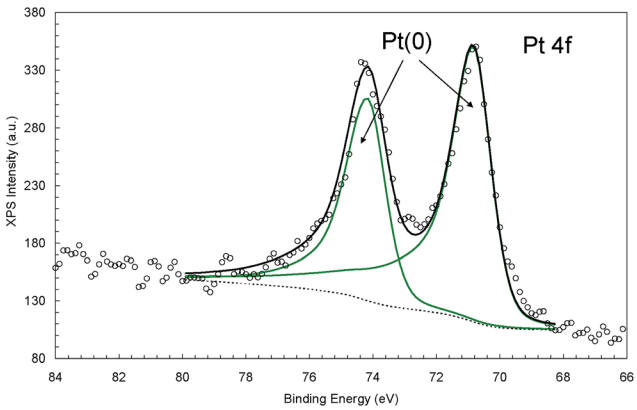

Fig. 3 XPS spectra of the Pt 4f obtained on Pt/Sb–SnO_2.

crystals. It might be possible that an interaction exists between Sn-metallic atoms and Pt-metallic atoms but the XPS method has not enough chemical sensitivity to prove this interaction directly.

The XPS spectra of Sb 3d and O 1s are shown in Fig. 4.

The Sb 3d spectra consist of doublet structure of $3d_{5/2}$ at 531.0 eV and $3d_{3/2}$ at 540.3 eV. Unfortunately, the main Sb $3d_{5/2}$ peak interferes strongly with the O 1s peak in the energy interval of 530–533 eV. We succeeded in decomposing the O 1s spectra into two components. The first component is at 530.9 eV and is related with O(2−) oxygen atoms in an oxide lattice structure. The second component is at 532.3 eV and is probably related to H_2O, OH or CO species on the surface.[28] The main differences between the non-treated and Pt-treated samples is that the Sb–SnO_2 sample contains a smaller contribution from adsorbed H_2O, OH or CO species (O 1s component at 532.3 eV) (Fig. 4a), whereas these species are much more present on the surface of Pt/Sb–SnO_2 (Fig. 4b). This may be also related to a much higher carbon C 1s signal present on these two samples. It is interesting to note that the Sb components are lower in the Pt/Sb–SnO_2 sample if compared to Sb+ in the SnO_2 sample. The binding energy of Sb $3d_{5/2}$ is at 531.0 eV, which indicates that the Sb-atoms are mainly in the (3+) oxidation state.[28]

TEM results revealed a homogenous Pt particle distribution, with an average particle size diameter of 2.9 nm.[24] The typical platinum particle clusters, as well as the FFT (Fast Fourier Transformation) of particles in the marked red square, taken close to [112] Pt zone axis are presented in Fig. 5.

3.2. Electrochemical characterization – the oxygen reduction reaction

A cyclic voltammogram recorded at the Pt/Sb–SnO_2 rotating disc electrode, as well as at the Sb–SnO_2 support (inset in Fig. 6), at 100 mV s^{-1} sweep rate, in the potential range from hydrogen to oxygen evolution is presented in Fig. 6.

The characteristic platinum shape for alkaline solutions can be seen, with three well defined peaks in the potential range of the underpotential deposition of hydrogen (from 0.03 V to 0.45 V *vs.* RHE). The electrochemically active surface area (EASA) of Pt, determined by the integration of the anodic part of the cyclic voltammogram in the potential range from 0.03 V to 0.45 V *vs.*

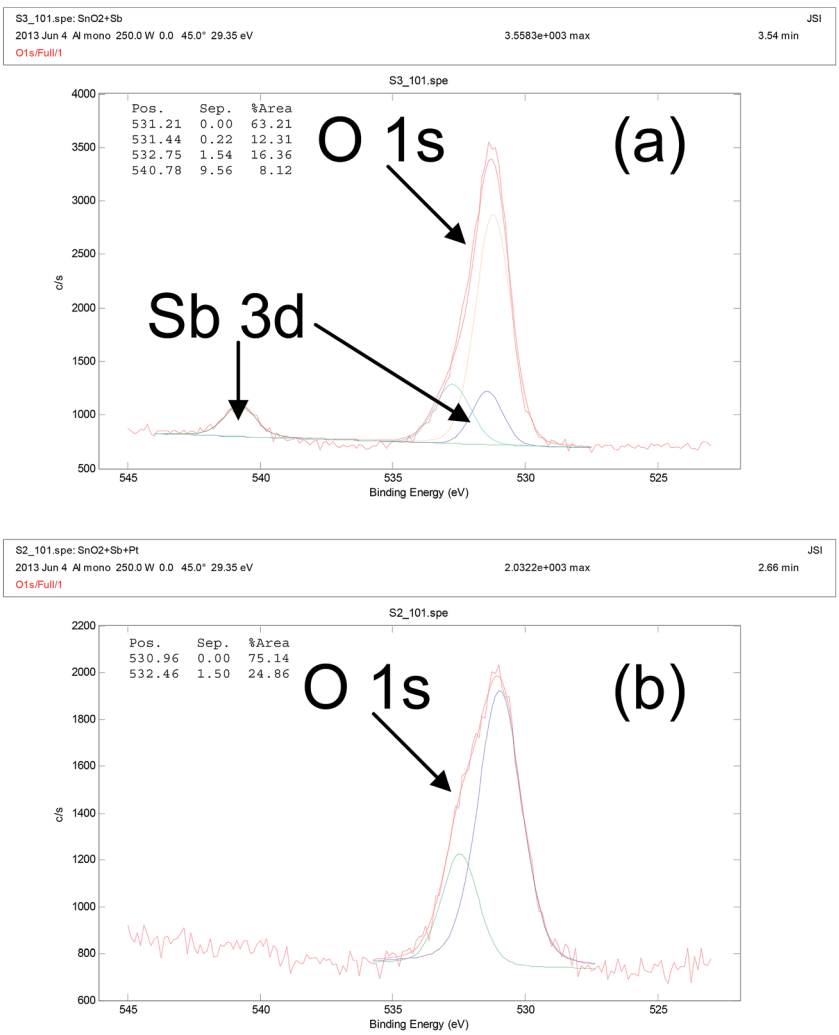

Fig. 4 XPS spectra of the Sb $3d_{5/2}$ and O 1s obtained on the Sb + SnO_2 sample (a) and Pt/Sb–SnO_2 sample (b).

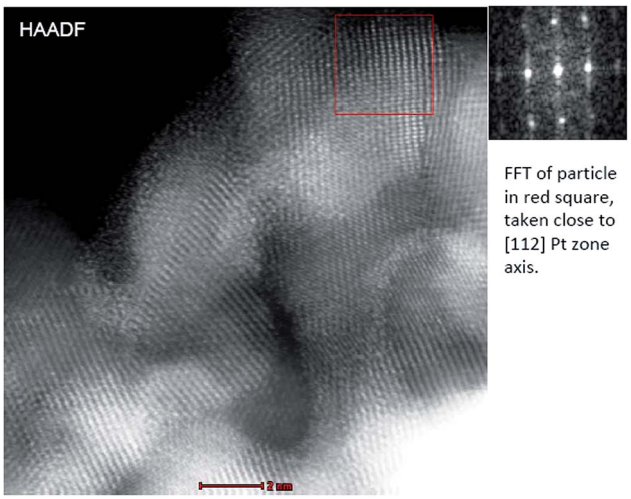

Fig. 5 HAADF image and the FFT of Pt particles cluster at Pt/Sb–SnO_2 catalyst.

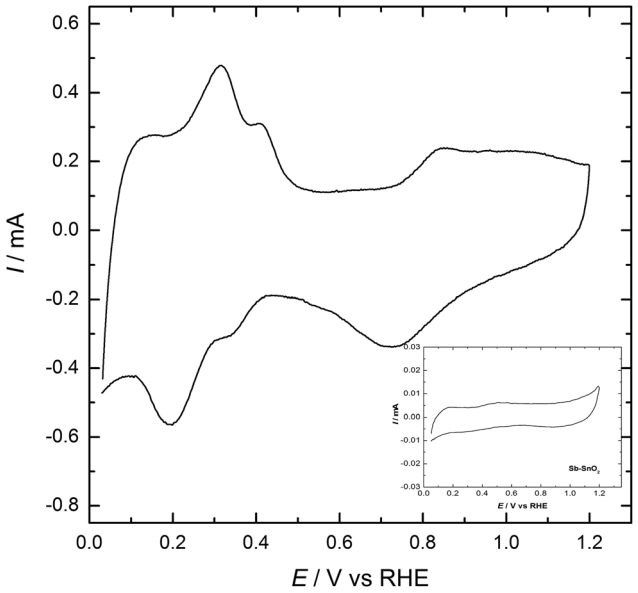

Fig. 6 Cyclic voltammograms obtained at Pt/Sb–SnO_2 and Sb–SnO_2 support, in 0.1 mol dm^{-3} NaOH at sweep rate of 100 mV s^{-1}, at 25 °C.

RHE, was 51 m^2 g^{-1}. This value is about 30% lower than the EASA determined at the Pt/Sb–SnO_2, by the same method, in acidic solution,[24] as it was expected for Pt based catalysts. The support was conductive and inert, with no electrochemical reactions taking place in this potential range, as it is clearly shown in the inset of Fig. 6. The cyclic voltammogram of the carbon supported Pt catalyst, used as benchmark, is shown in Fig. 7.

The oxygen reduction reaction was investigated by linear sweep voltammetry, at the sweep rate of 20 mV s^{-1}, at different rotation rates. The polarization curves, obtained by positive sweep, are presented in Fig. 8.

It can be seen that well defined diffusion limiting current densities were obtained, close to the corresponding theoretical values for the same electrolyte and rotation rates, expressed per

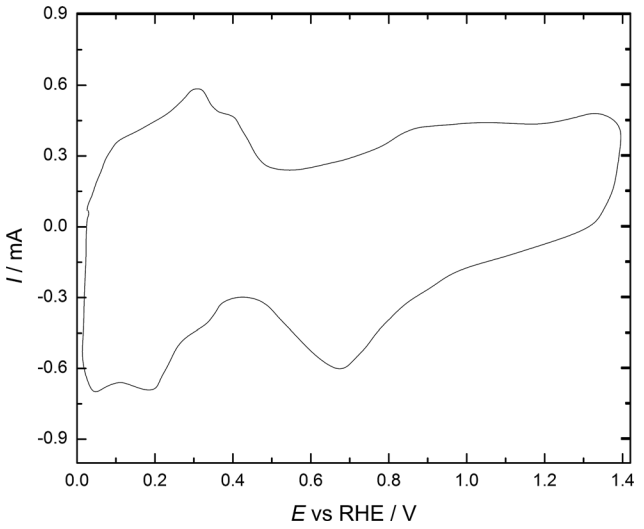

Fig. 7 Cyclic voltammogram obtained at Pt/C catalyst, in 0.1 mol dm^{-3} NaOH at a sweep rate of 100 mV s^{-1}, at 25 °C.

geometric surface area of the electrode. This fact is the indication of proper Pt loading per geometric surface area for rotating disc electrode measurements.[29]

As the oxygen reduction belongs to the mixed control processes, the total current density can be expressed by Lewich–Koutecky equation:

$$j^{-1} = j_k{}^{-1} + (B\omega^{1/2})^{-1} \quad (2)$$

The measured total current density (j) is the function of the kinetic current density (j_k) and diffusion limiting current density ($j_D = B\omega^{1/2}$), and B is defined by following equation:

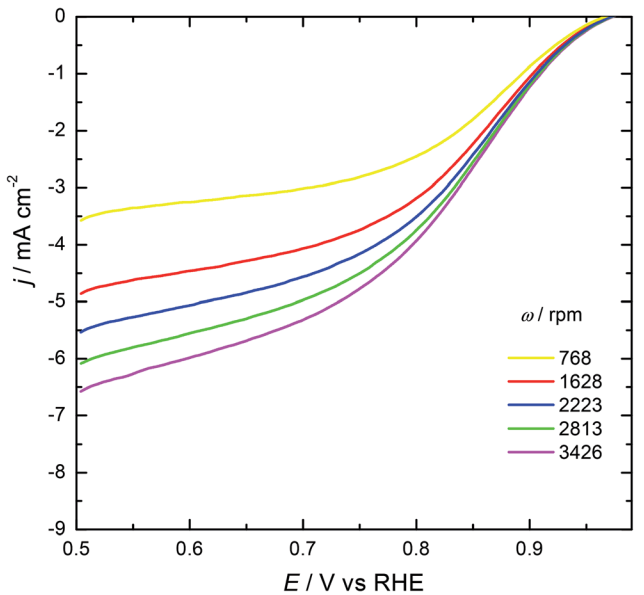

Fig. 8 Polarization curves for oxygen reduction at Pt/Sb–SnO_2 catalyst in 0.1 mol dm^{-3} NaOH at sweep rate of 20 mV s^{-1}, at 25 °C. Currents densities are presented per geometric surface area of the electrode.

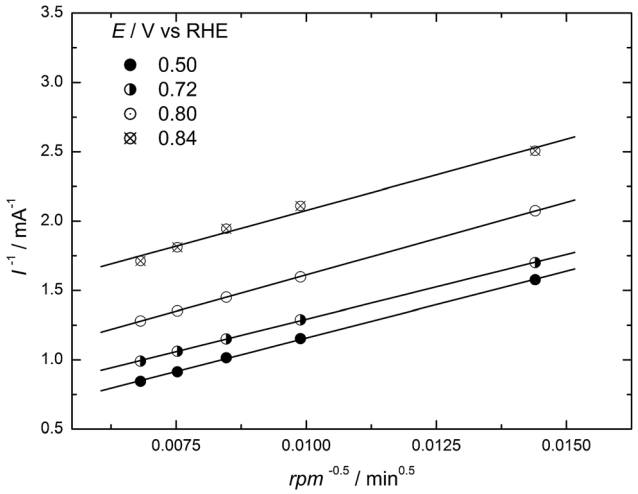

Fig. 9 Levich–Koutecky dependence obtained at Pt/Sb–SnO_2 electrode in 0.1 mol dm^{-3} NaOH.

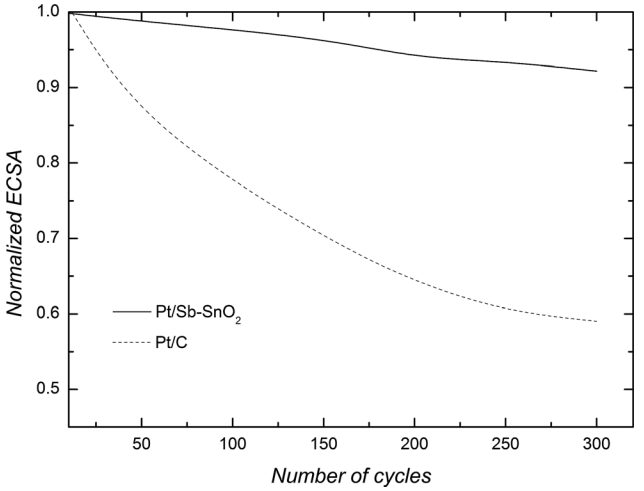

Fig. 11 Dependence of normalized EASA on the cycle number for Pt/Sb–SnO_2 and Pt/C catalysts.

$$B = 0.620nFC_{O_2}D_{O_2}^{2/3}\nu^{-1/6} \quad (3)$$

Taking into account previously reported values[30] for the constants in eqn (3) for 0.1 mol dm^{-3} NaOH solution: D_{O_2} – diffusion coefficient of oxygen (2.22×10^{-5} cm^2 s^{-1}), ν – the kinematics viscosity of the solution (1.1×10^{-2} cm^2 s^{-1}) and C_{O_2} – the bulk concentration of dissolved oxygen molecules (1.13×10^{-6} mol cm^{-3}), the number of electrons exchanged close to four was calculated from Levich–Koutecky dependence (Fig. 9).

The kinetic current densities at each potential value can be determined from the intercept of Levich–Koutecky dependence (Fig. 9), j *vs.* $\omega^{-1/2}$. The mass transfer currents contribution corrected Tafel plot is presented in Fig. 10.

According to previously published studies, the Tafel slope values for oxygen reduction at bulk platinum catalysts in alkaline solution should be close to -60 mV dec^{-1} at low current densities, and -120 mV dec^{-1} in the potential region of high current densities.[31,32] Experimentally obtained Tafel slope values: -0.056 V dec^{-1} and -0.119 V dec^{-1} are in good accordance to the already accepted reported values.

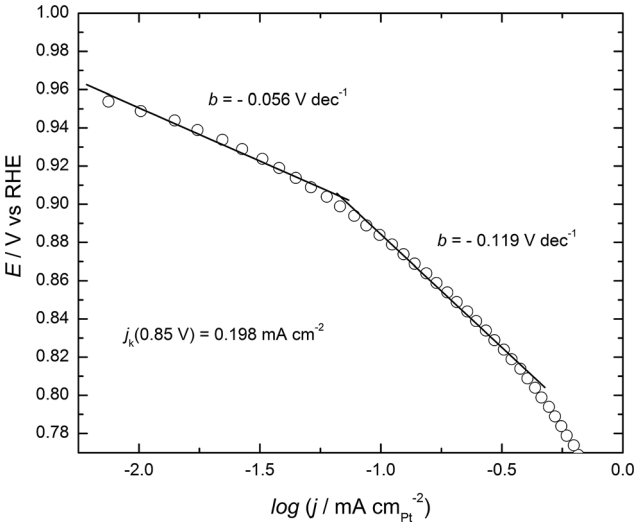

Fig. 10 Tafel plots for oxygen reduction reaction at Pt/Sb + SnO_2 catalyst, in 0.1 mol dm^{-3} NaOH.

It is common to compare catalytic activities for oxygen reduction at Pt based catalysts at 0.85 V *vs.* RHE, where the mass contribution current can be considered as negligible. The obtained kinetic current density value of 0.198 mA cm^{-2} (Fig. 10) is in good accordance to the corresponding value at Pt catalyst on carbon based support, obtained at the same experimental conditions.[33]

The stability and durability of the catalyst were investigated by repetitive cycling in the potential region from 0 V to 1.4 V *vs.* RHE. Cyclic voltammograms obtained after repetitive cycling was integrated in the potential region of underpotential deposition of hydrogen and the obtained charge amount was divided by that initially obtained. The dependence of determined normalized electrochemically active surface area on the cycle number is presented in Fig. 11. The stability test proved clearly the advantage of the Pt catalyst on the Sb–SnO_2 support over the carbon supported one.

Having in mind the already referred to and widely accepted disadvantages of carbon based supports,[15,16] and the results obtained in this study, the benefit of Sb–SnO_2 application is clear. Although the comparable catalytic values, in comparison to carbon supported one were determined, synthesized Pt catalyst on the new tin oxide based support material exhibited better stability at high anodic potentials. It makes this catalyst promising as a fuel cell cathode to overcome carbon based supports durability disadvantages.

4. Conclusion

An antimony doped SnO_2 support to be used as a support for Pt catalysts was successfully synthesized by a modified hydrazine reduction. XPS spectra revealed that the Pt-deposition on the Sb–SnO_2 support induced reduction of the Sn(4+) oxidation

state to Sn(2+) and Sn(0) states, while Pt remained in the metallic state. Sb was in the (3+) oxidation state. HRTEM analysis revealed a homogenous platinum particle distribution over the Sb–SnO_2 support.

The electrochemically determined active surface area of Pt was 51 m^2 g^{-1}. The determined catalytic activity for oxygen reduction, expressed in terms of kinetic current density per real Pt surface area at the constant potential value of 0.85 V *vs.* RHE was 0.198 mA cm^{-2}, whereas the corresponding mass activity was 101 mA mg_{Pt}^{-1}. The testing of the catalyst's stability and durability proved the benefit of this catalyst for long term application.

Acknowledgements

This study was financially supported by the Ministry of Education, the Science and Technological Development Republic of Serbia, under contract no. 172054. We acknowledge the support for XPS measurements from the Jozef Stefan Institute, Ljubljana, Slovenia, under bilateral collaboration project, contact no 451-03-3095/2014-09/26. Electron microscopy characterization was performed at the National Center for Electron Microscopy, Lawrence Berkeley National Laboratory, which is supported by the Office of Science, Office of Basic Energy Sciences, of the U.S. Department of Energy under Contract no. DE-AC02-05CH11231. V. R. Radmilovic acknowledges the supports from the Serbian Academy of Sciences and Arts.

References

1 J. S. Spendelov and A. Wieckowski, *Phys. Chem. Chem. Phys.*, 2007, **9**, 2654–2675.
2 G. F. McLean, T. Niet, S. Prince-Richard and N. Djilali, *Int. J. Hydrogen Energy*, 2002, **27**, 507–526.
3 J. R. Varcoe and R. C. T. Slade, *Electrochem. Commun.*, 2006, **8**, 839–843.
4 N. M. Markovic and P. N. Ross, *Surf. Sci. Rep.*, 2002, **45**, 121–229.
5 X. Li, B. N. Popov, T. Kawaharab and H. Yanagib, *J. Power Sources*, 2011, **196**, 1717–1722.
6 M. Li, L. Q. Jiang, L. Lin, Y. F. Li, D. L. Yu, L. L. Cui and X. Q. He, *J. Solid State Electrochem.*, 2014, **18**, 2743–2753.
7 A. Nakamura, H. Takahashi, T. Takeguchi, T. Yamanaka, Q. Wang, Y. Uchimoto and W. Ueda, *ECS Trans.*, 2010, **28**, 153–158.
8 L. Xu, G. Pan and X. Liang, *RSC Adv.*, 2014, **4**, 19756–19765.
9 X. Wang, H. Fu, W. Li, J. Zheng and X. Li, *RSC Adv.*, 2014, **4**, 37779–37785.
10 Y. S. Wang, B. Zhang, Y. F. Li, D. J. Liu, X. He and Z. J. Si, *RSC Adv.*, 2014, **4**, 62272–62280.
11 N. M. Markovic, H. A. Gasteiger and P. N. Ross, *J. Phys. Chem.*, 1996, **100**, 6715–6721.
12 F. H. B. Lima, J. Zhang, M. H. Shao, K. Sasaki, M. B. Vukmirovic, E. A. Ticianelli and R. Adzic, *J. Phys. Chem. C*, 2007, **111**, 404–410.
13 K. Tammeveski, T. Teno, J. Claret and C. Ferrater, *Electrochim. Acta*, 1997, **42**, 893–897.
14 N. Alexeyeva, K. Tammeveski, A. Lopez-Cudero, J. Solla-Gullón and J. M. Feliu, *Electrochim. Acta*, 2010, **55**, 794–803.
15 C. A. Reiser, L. Bregoli, T. W. Patterson, J. S. Yi, J. D. Yang, M. L. Perry and T. D. Jarvi, *Electrochem. Solid-State Lett.*, 2005, **8**, A273–A276.
16 L. M. Roen, C. H. Paik and T. D. Jarvi, *Electrochem. Solid-State Lett.*, 2004, **7**, A19–A22.
17 K. Tammeveski, T. Tenno, A. Rosental, P. Talonen, L. S. Johansson and L. Niinistö, *J. Electrochem. Soc.*, 1999, **146**, 669–676.
18 K. Tiido, N. Alexeyeva, M. Couillard, C. Bock, B. R. MacDougall and K. Tammeveski, *Electrochim. Acta*, 2013, **107**, 509–517.
19 K. S. Lee, I. S. Park, Y. H. Cho, D. S. Jung, N. Jung, H. Y. Park and Y. E. Sung, *J. Catal.*, 2008, **258**, 143–152.
20 A. Masao, S. Noda, F. Takasaki, K. Ito and K. Sasaki, *Electrochem. Solid-State Lett.*, 2009, **12**, B119–B122.
21 F. Takasaki, S. Matsuie, Y. Takabatake, Z. Noda, A. Hayashi, Y. Shiratori, K. Ito and K. Sasaki, *J. Electrochem. Soc.*, 2011, **158**, B1270–B1275.
22 F. Takasaki, Z. Noda, A. Masao, Y. Shiratori, K. Ito and K. Sasaki, *ECS Trans.*, 2009, **25**, 831–838.
23 A. Hagemeyer, Z. Hogan, M. Schlicher, B. Smaka, G. Streukens, H. Turner, A. Volpe, J. H. Weinberg and K. Yaccato, *Appl. Catal., A*, 2007, **317**, 139–148.
24 N. R. Elezović, B. M. Babić, V. R. Radmilović and N. V. Krstajić, *J. Electrochem. Soc.*, 2013, **160**, F1151–F1158.
25 K. W. Park and K. S. Seul, *Electrochem. Commun.*, 2007, **9**, 2256–2260.
26 W. P. Zhou, S. A. Michael, G. White, R. Adzic and J. Hrbek, *J. Phys. Chem. C*, 2011, **115**, 16467–16473.
27 W. Z. Hung, W. H. Chung, D. S. Tsai, D. P. Wilkinson and Y. P. Huang, *Electrochim. Acta*, 2010, **55**, 2116–2122.
28 J. F. Moulder, W. F. Stickle, P. E. Sobol and K. D. Bomben, *Handbook of X-Ray Photoelectron Spectroscopy*, Physical Electronics Inc., Eden Prairie, Minnesota, USA, 1995.
29 K. J. J. Mayrhofer, D. Strmcnik, B. B. Blizanac, V. Stamenkovic, M. Arenz and N. M. Markovic, *Electrochim. Acta*, 2008, **53**, 3181–3188.
30 R. C. Weastled, *Handbook of Chemistry and Physics*, C.R.C Press, Cleveland, Ohio, 55th edn, 1984.
31 A. Damjanovic, M. A. Genshaw and J. O. 'M. Bockris, *J. Electrochem. Soc.*, 1967, **114**, 1107–1112.
32 N. M. Markovic, H. A. Gasteiger and P. N. Ross, *J. Phys. Chem.*, 1996, **100**, 6715–6721.
33 N. R. Elezovic, B. M. Babic, Lj. M. Gajic-Krstajic, P. Ercius, V. R. Radmilovic, N. V. Krstajic and Lj. M. Vracar, *Electrochim. Acta*, 2012, **69**, 239–246.